nature plants

ARTICLES

https://doi.org/10.1038/s41477-021-00947-5

Impact of ion fluxes across thylakoid membranes on photosynthetic electron transport and photoprotection

Meng Li[1,5], Vaclav Svoboda[1], Geoffry Davis[2], David Kramer[2,3], Hans-Henning Kunz[4] and Helmut Kirchhoff[1]✉

In photosynthetic thylakoid membranes the proton motive force (pmf) not only drives ATP synthesis, in addition it is central to controlling and regulating energy conversion. As a consequence, dynamic fine-tuning of the two pmf components, electrical (Δψ) and chemical (ΔpH), is an essential element for adjusting photosynthetic light reactions to changing environmental conditions. Good evidence exists that the Δψ/ΔpH partitioning is controlled by thylakoid potassium and chloride ion transporters and channels. However, a detailed mechanistic understanding of how these thylakoid ion transporter/channels control pmf partitioning is lacking. Here, we combined functional measurements on potassium and chloride ion transporter and channel loss-of-function mutants with extended mathematical simulations of photosynthetic light reactions in thylakoid membranes to obtain detailed kinetic insights into the complex interrelationship between membrane energization and ion fluxes across thylakoid membranes. The data reveal that potassium and chloride fluxes in the thylakoid lumen determined by the K^+/H^+ antiporter KEA3 and the voltage-gated Cl^- channel VCCN1/Best1 have distinct kinetic responses that lead to characteristic and light-intensity-dependent Δψ/ΔpH oscillations. These oscillations fine-tune photoprotective mechanisms and electron transport which are particularly important during the first minutes of illumination and under fluctuating light conditions. By employing the predictive power of the model, we unravelled the functional consequences of changes in KEA3 and VCCN1 abundance and regulatory/enzymatic parameters on membrane energization and photoprotection.

A ubiquitous principal of biological energy conversion is transient energy storage as a proton motive force (pmf) across a proton-sealed membrane that is employed by ATP synthases for generation of the more stable and universal energy equivalent ATP from ADP and inorganic phosphate[1–3]. Because protons carry a charge, the pmf is the sum of two components: one electrical (Δψ) and one chemical (ΔpH). Both are equivalent in driving ATP synthesis at the ATPase enzyme[4]. Whereas in respiratory membranes the pmf is mainly stored as Δψ, for a long time it was assumed that the Δψ under steady-state illumination is small in photosynthetic thylakoid membranes and the pmf consists mainly of ΔpH[5]. This view of thylakoid pmf storage has been challenged by improved spectroscopic analyses[6–9] that disentangle the contributions of ΔpH and Δψ to total pmf storage, combined with the identification and characterization of thylakoid ion channel/transporters mutants, implicating storage of a fraction of pmf as Δψ. An explanation of the controversy about pmf partitioning in thylakoid membranes is that the ΔpH/Δψ ratio is not static but dynamic and could depend on environmental/metabolic conditions in vivo (for example ref. [10]), as well as the experimental conditions under which it is measured[8]. The attractiveness of dynamic pmf partitioning is that it enables fine-tuning of photosynthetic electron transport and light harvesting without compromising ATP synthesis. This is based on the fact that the main regulatory processes in thylakoid membranes are dependent on ΔpH (more precisely on the acidity of the thylakoid lumen) but not Δψ. In detail, proton-releasing reactions in the thylakoid lumen, water splitting at photosystem II (PSII) and plastoquinol oxidation at the cytochrome b_6f (cyt b_6f) complex, are slowed by lumen acidification in light (high ΔpH)[11,12], a phenomenon called photosynthetic control. Furthermore, the photoprotective non-photochemical quenching mechanism (NPQ, more precisely the dominating high-energy-quenching component (qE)) localized mainly in the thylakoid-hosted light-harvesting complexes II is activated and triggered at high ΔpH[13–15]. Therefore, pmf redistribution from the Δψ component to the ΔpH component would downregulate light harvesting (NPQ) and electron transport (photosynthetic control) but leave ATPase activity unaffected[9,16]. How can pmf partitioning be adjusted? Here, thylakoid membrane ion channels and transporters come into play. The main ions in chloroplasts are potassium (K^+) and chloride (Cl^-)[17,18]. ΔpH/Δψ partitioning can be tuned by the pmf-driven passive influx of Cl^- into the thylakoid lumen and/or by K^+/H^+ antiport (K^+ in, H^+ out). The influx of Cl^- into the lumen is expected to decrease Δψ (charge compensation in the lumen) allowing an increase in ΔpH (at constant pmf), whereas a K^+/H^+ antiport is expected to decrease ΔpH allowing an increase in Δψ. Early evidence from electrophysiological measurements suggesting the existence of K^+ and Cl^- channels or transporters in thylakoid membranes[19,20] was recently validated by molecular biological studies (see reviews [21,22]). At present, bona fide thylakoid channels/transporters are the K^+/H^+ antiporter KEA3 (ref. [23]), the voltage-gated Cl^- channel VCCN1/Best1 (refs. [24,25]) and the Cl^- channel ClCe[26,27]. A few years ago, the

[1]Institute of Biological Chemistry, Washington State University, Pullman, WA, USA. [2]Department of Energy Plant Research Laboratory, Michigan State University, East Lansing, MI, USA. [3]Department of Biochemistry, Michigan State University, East Lansing, MI, USA. [4]School of Biological Sciences, Washington State University, Pullman, WA, USA. [5]Present address: School of Oceanography, University of Washington, Seattle, WA, USA. ✉e-mail: kirchhh@wsu.edu

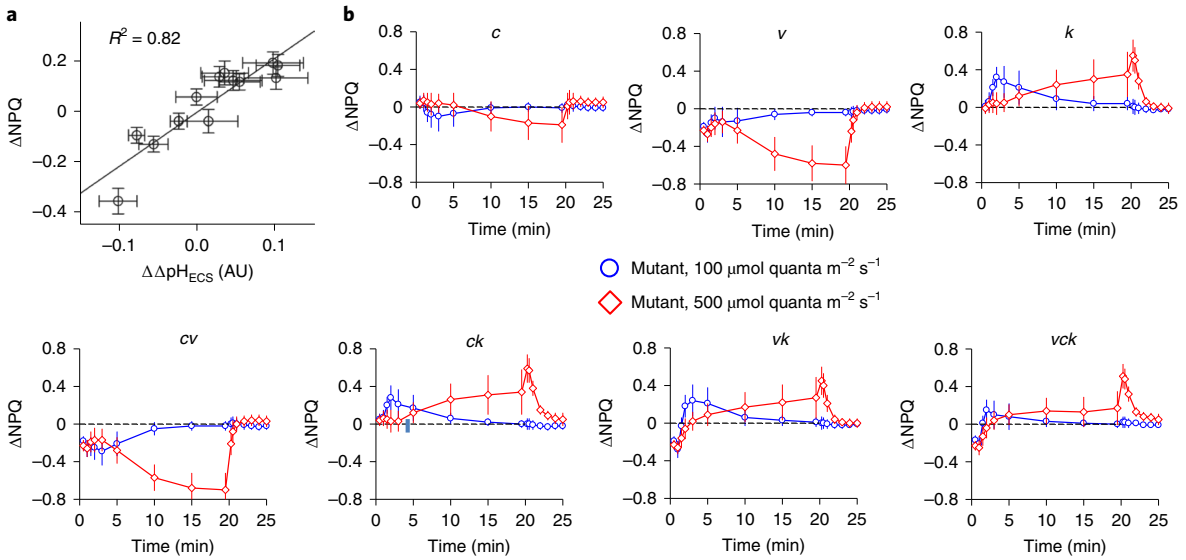

Fig. 1 | NPQ characteristics in KEA3, VCCN1 and Clce mutants. a, Correlation between NPQ changes in all mutants ($\Delta NPQ = NPQ_{mutant} - NPQ_{WT}$) versus corresponding changes in the pH component of the ECS (ΔpH_{ECS}). Data are also represented as the difference of mutant minus WT ($\Delta\Delta pH_{ECS} = \Delta pH_{ECS,\,mutant} - \Delta pH_{ECS,\,WT}$). Both parameters were measured on intact leaves. Data were taken after an average of 7.5 min illumination with 500 μmol quanta m^{-2} s^{-1}. **b**, Difference in NPQ ($\Delta NPQ = NPQ_{mutant} - NPQ_{WT}$) for two light intensities (100 and 500 μmol quanta m^{-2} s^{-1}) measured on intact plants. Light was turned on at 0 min and off at 20 min. Data show the mean of *n* (WT, *c*, *v*, *k*, *cv*, *ck*, *vk*, *vck*) = (16, 26, 14, 14, 14, 13, 15, 13) plants with standard deviation. AU, arbitrary units.

two-pore K^+ channel TPK3 was suggested as another thylakoid channel[28]. However, newer detailed studies make genuine chloroplast localization unlikely[29–31]. Although good characterizations of these thylakoid ion transporter/channels concerning sublocalization, molecular biological characterization and their implication in fine-tuning photosynthetic energy conversion exist,[21,22,32] a mechanistic understanding of how they determine ion fluxes, ΔpH and Δψ across thylakoid membranes, both individually and in concert, is missing. This lack of a mechanistic understanding is, to some degree, due to the methodical challenge of measuring ion fluxes across thylakoid membranes in vivo. Here, we take an alternative approach to this challenge by combining measured photosynthetic parameters of thylakoid ion transporter/channel loss-of-function mutants with a computer model for photosynthetic light reactions that includes fluxes through thylakoid transporter/channels. The computer model is an extension of a recently published version[9].

Results

Growth phenotype and characterization of thylakoid ion channel/transporter mutants. For characterization of ion fluxes over thylakoid membranes by KEA3, VCCN1 and ClCe transporter/channels, single and multiple loss-of-function mutants were generated. The single knockout mutants, *kea3-1* (ref. [23]), *vccn1-1* (SALK_103612C)[25] and *clce-2* (Salk_010237)[26], were used to generate homozygous double mutants, *clce-2kea3-1* (*ck*), *clce-2vccn1-1* (*cv*) and *vccn1-1kea3-1* (*vk*), and the triple mutant, *vccn1-1clce-2kea3-1* (*vck*) (Supplementary Fig. 1). The composition of key thylakoid membrane components reveals that the abundance of the proteins light-harvesting complexes II, PSII, photosystem I, cyt b_6f complex, ATPase and PsbS, as well as carotenoids, is very similar in all eight genotypes (Supplementary Fig. 2). It was reported that thylakoid ion transporter/channel mutants show functional phenotypes mainly under fluctuating light conditions[25,33,34]. To examine how fluctuating light intensities affect plant growth, total leaf areas were determined by plant imaging under constant and fluctuating light regimes (Supplementary Fig. 3). Only mutants that lack KEA3 antiport activity show statistically significant reduced growth and only under fluctuating light conditions (Supplementary Fig. 3), in accordance with recently published data[32].

Because it is expected that altered ion fluxes across the thylakoid membrane in ion transporter/channel mutants affect membrane energization, ΔpH was examined in vivo. In the following, we express parameter changes in mutants as difference from wild-type (WT) plants (that is mutant minus WT) because this focuses directly on alterations caused by the mutation. A readily quantifiable proxy for ΔpH across thylakoid membranes is NPQ[35]. However, NPQ also depends on the PsbS protein and the xanthophyll zeaxanthin[14,15,36]. As mentioned above, neither PsbS level nor xanthophyll pool size is different in the mutants compared with WT (Supplementary Fig. 2) providing justification for the use of NPQ as a qualitative measure of ΔpH. To further validate the NPQ parameter as a proxy for ΔpH, we measured the electrochromic shift signal (ECS) on dark-adapted intact leaves. From ECS signals, total pmf, as well as the Δψ ($\Delta\psi_{ECS}$) and ΔpH (ΔpH_{ECS}) components can be extracted[4,37,38]. Experiments using the ΔpH indicator 9-aminoacridine (9-AA[39,40]) on fresh isolated intact isolated thylakoid membranes confirm that ΔpH_{ECS} measures ΔpH (Supplementary Fig. 4). Figure 1a shows plots of ΔNPQ versus $\Delta\Delta pH_{ECS}$ (mutant minus WT) with 7.5 minutes of illumination. The good correlation supports that ΔNPQ can indeed be used as a proxy for ΔpH changes.

Figure 1b summarizes ΔNPQ changes for growth (100 μmol quanta m^{-2} s^{-1}) and elevated (500 μmol quanta m^{-2} s^{-1}) light intensities (for original NPQ kinetics see Supplementary Fig. 5). The ΔNPQ behaviours of the mutants are strikingly different. (1) A general trend is that NPQ was lower in mutants lacking either of the two functional chloride channels, whereas it was higher in the absence of the K^+/H^+ antiporter KEA3, consistent with each proposed function in redistributing ΔpH/Δψ. (2) ClCe had less impact on lowering NPQ than VCCN1. (3) During illumination, mutants without KEA3 (*k*, *ck*, *vk*, *vck*) showed a characteristic transient increase in NPQ at around 2 min at 100 μmol quanta m^{-2} s^{-1}. (4) For the same light intensity, the *vccn1* mutant showed a fast (< 1 min) transient decline in ΔNPQ. (5) For longer time points (>10 min), NPQ relaxed completely to WT levels at the lower light intensity in

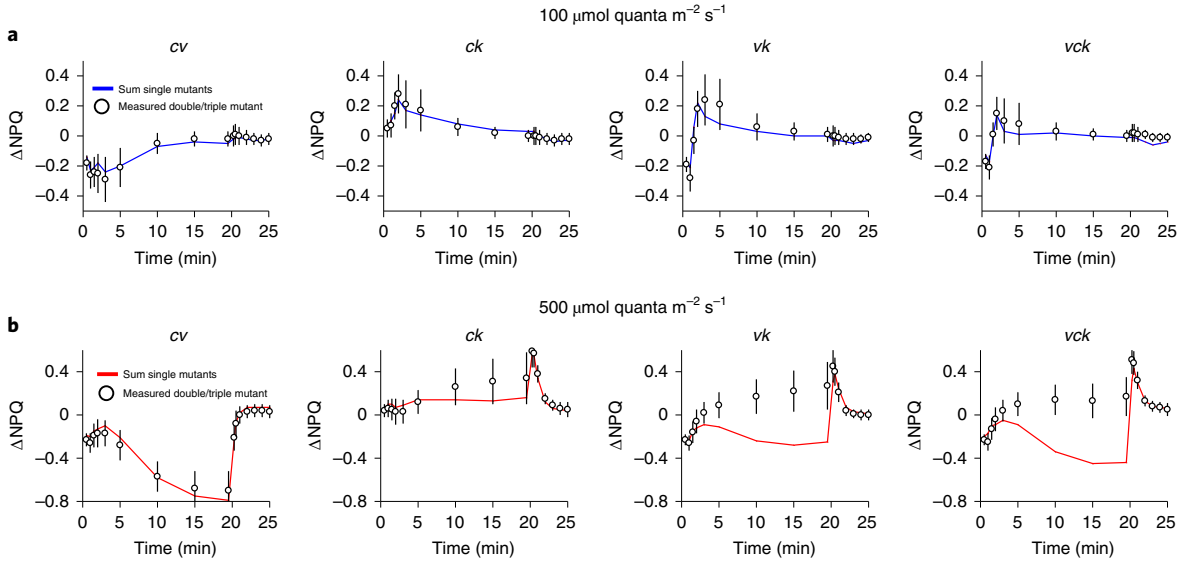

Fig. 2 | Testing the independence of KEA3, VCCN1 and ClCe functionality. The graphs show the measured ΔNPQ for the double and triple mutants (circles) compared with their mathematical sum of the single mutants (lines). Independent functionality is indicated if the sum of single mutants equals the data for double and triple mutants. **a**, Results for 100 µmol quanta m^{-2} s^{-1}. **b**, Results for 500 µmol quanta m^{-2} s^{-1}. Data show the mean of *n* (WT, *c*, *v*, *k*, *cv*, *ck*, *vk*, *vck*) = (16, 26, 14, 14, 14, 13, 15, 13) plants with standard deviation.

all mutants, indicative of transient changes in ΔpH and ion fluxes at 100 µmol quanta m^{-2} s^{-1}. (6) In contrast, at 500 µmol quanta m^{-2} s^{-1}, a larger difference in ΔNPQ appeared over the 20 min illumination period, with decreases in *v*-mutants and increases in *k*-mutants likely pointing to sustained changes in ion fluxes and ΔpH at higher light or the involvement of other non-photochemical quenching types (see below). (7) All mutants without KEA3 showed slower NPQ relaxations at 500 µmol quanta m^{-2} s^{-1} visualized as a positive ΔNPQ spike after light off (20 min). For shorter periods (<10 min) the ΔNPQ changes measured in Fig. 1 are in accordance with published data for VCCN1 (refs. [25,32]), KEA3 (refs. [34,35]) and the higher-order mutants[29,32]. To date, no results have been published for periods >10 minutes.

Do thylakoid ion transporter/channels operate independently from each other? The availability of higher-order ion transporter/channel mutants allows the possibility of examining whether the transport proteins operate independently in thylakoid membranes. Independent operation of channels/transporters would be visible as a similar behaviour of measured higher-order mutants compared with the sum of their corresponding single mutants, whereas deviation between the two indicates that channels/transports function non-independently. The latter could be explained by compensatory ion fluxes triggered by loss of function of a certain channel/transporter. In a recent study on thylakoid ion transporter/channels it was concluded that the three transporter/channels studied here work independently[32]. The ΔNPQ results in Fig. 2 confirm this independency for 100 µmol quanta m^{-2} s^{-1} (Fig. 2, upper panel); that is, the ΔNPQ change in higher-order mutants is the sum of respective single mutants. However, for 500 µmol quanta m^{-2} s^{-1} a different conclusion must be drawn. Although the chloride channel double-mutant *cv* shows clear indications of the independent operation of ClCe and VCCN1, the data for higher-order *kea3* mutants reveal that the behaviour in double and triple mutants deviates clearly from the sum of the single mutant for illumination times >3 min (Fig. 2 bottom panel). The data indicate that at higher light intensities, the ΔNPQ phenotype is dominated by the absence of KEA3 (measured data are more positive than the sum of single mutants).

Validation of a computer model simulating photosynthetic light reactions. Because ion fluxes, electron transport, proton pumping and thylakoid membrane energization form a complex, highly interwoven and dynamic functional network, it is difficult to comprehend the consequences of altered ion fluxes in thylakoid channel/transporter mutants on these parameters. To obtain mechanistic insights into the functional consequences of altered ion fluxes, we modified a recently published computer model[9] that describes light harvesting, electron transport, proton pumping, ATP synthesis, NPQ, ion fluxes and ATP/NADPH consumption in the Calvin–Benson cycle (Fig. 3a) by employing coupled differential equations. Rate constants, stoichiometries, pH dependencies and enzyme activities of individual reactions required for the modelling were taken from the literature. Details of the model are given in Supplementary Fig. 6 and Supplementary Methods. Owing to substantial progress over past decades, good quantitative values are available for many model parameters (Supplementary Methods). However, the best way to build up confidence in a model is to test its outcomes by experiments. As a first step, we compared measured kinetics of chlorophyll (Chl) fluorescence parameters qL (fraction of open PSII centres), ΦII (operating efficiency of PSII) and NPQ for WT plants (Fig. 3b) with the outcome of the model. All three measuring parameters were well described by the model for 100 µmol quanta m^{-2} s^{-1} (black curves and symbols). The modelled NPQ amplitude for 500 µmol quanta m^{-2} s^{-1} was slightly lower and the relaxation was faster than measured. This may be explained by the fact that the model does not include slower NPQ components such as qZ or qI that can contribute notable at higher light intensities[41,42]; that is, the model assumes that NPQ is entirely the high-energy quenching part qE. As a consequence of the ~15% lower NPQ in the model for 500 µmol quanta m^{-2} s^{-1}, the ΦII parameter, which is a measure of linear electron transport, is slightly higher compared with the measured data. Including qZ and qI in the model is not straightforward and the gain for the model is limited. Therefore, we decided not to model qZ and qI. The second comparison between the model and the experiment was the ΔΔpH changes in the mutants relative to WT for the two light intensities examined (Fig. 3c). The model predicts the right direction of the changes and for many mutants is quantitatively correct (within the

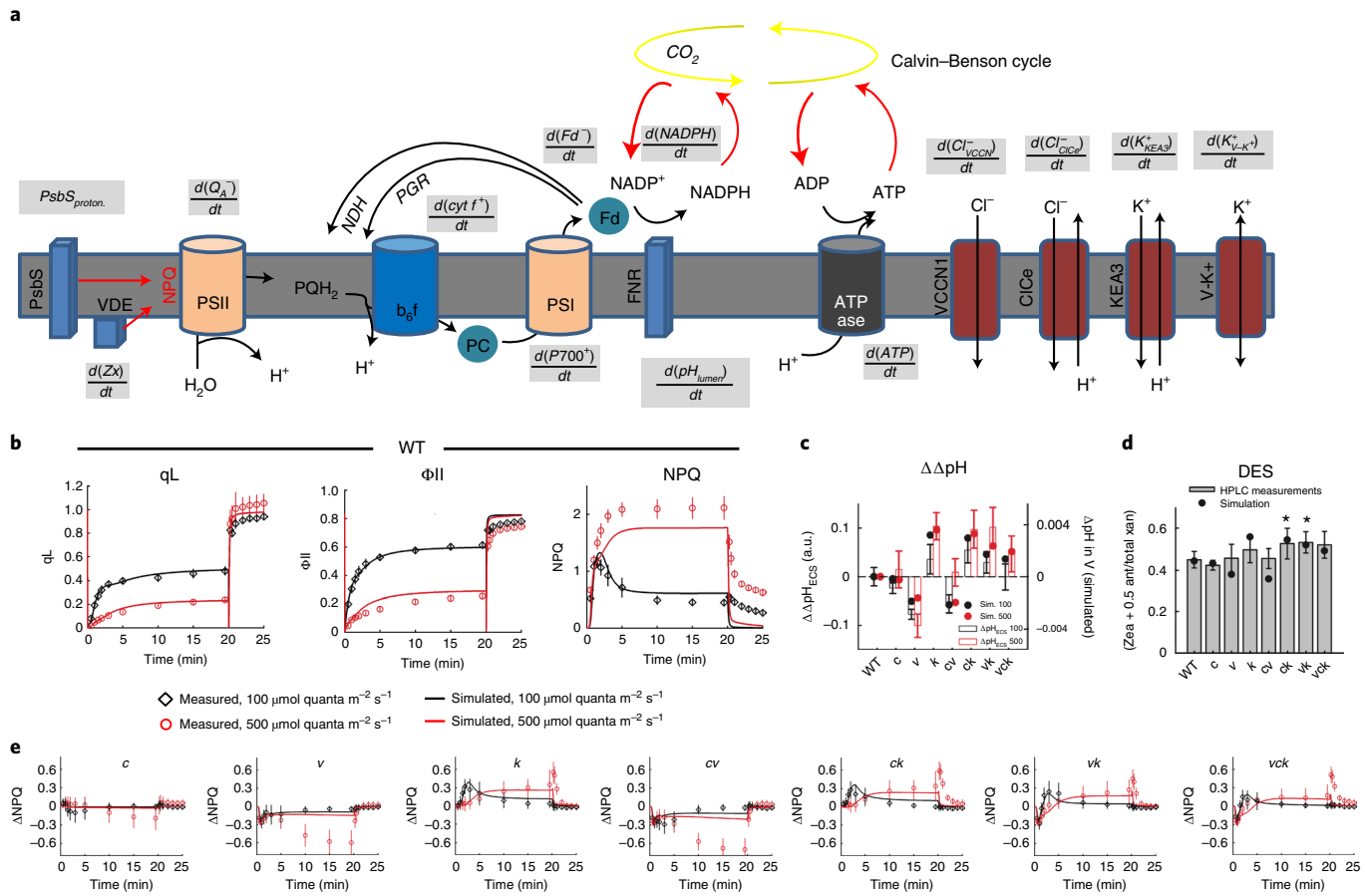

Fig. 3 | Computer model of photosynthetic light harvesting coupled to CO_2 fixation in the Calvin–Benson cycle. a, Cartoon summarizing the model parameters. Electron, proton, ion and metabolite fluxes are expressed by differential equations that are defined in Supplementary Fig. 6. **b**, Comparison of modelled and measured qL, ΦII and NPQ data for WT for 100 and 500 µmol quanta m^{-2} s^{-1}. **c**, Comparison of modelled and measured ΔΔpH changes. **d**, Comparison of modelled and measured changes in the de-epoxidation status of the xanthophyll pool for 500 µmol quanta m^{-2} s^{-1}. Asterisks indicate statistically significant changes (two-sided Student's *t*-test, for *ck*: $P = 0.0362$; for *vk*: $P = 0.0179$). **e**, Comparison of modelled and measured ΔNPQ for all ion transporter and channel mutants. Data in **b** and **e** show the mean with standard deviation of *n* (WT, *c*, *v*, *k*, *cv*, *ck*, *vk*, *vck*) = (16, 26, 14, 14, 14, 13, 15, 13) biological independent samples. Data in **c** show the mean with standard deviation of $n = 16$ biological independent samples. Data in **d** show the mean with standard deviation of $n = 9$ biological independent samples. DES, de-expoxidation state; HPLC, high-performance liquid chromatography; PGR, proton gradient regulation 5; VDE, violaxanthin deepoxidase.

range of experimental deviation). Furthermore, the de-epoxidation state of the xanthophyll pool measured for leaves illuminated with 500 µmol quanta m^{-2} s^{-1} light intensity is predicted quantitatively by our simulations (Fig. 3d). The 100 µmol quanta m^{-2} s^{-1} light intensity was not examined because the de-epoxidation state is very low at this light intensity due to low violaxanthin–de-epoxidase activity. Finally, model performance was tested by its prediction of ΔNPQ changes (Fig. 3e). Good agreement between simulated and measured ΔNPQ kinetics is apparent with the exception that it fails to simulate the measured slow ΔNPQ decline (>5 min) in the *v* and *cv* mutants at 500 µmol quanta m^{-2} s^{-1}. One possibility is that the slow ΔNPQ decline reflects qZ or qI, which are not included in the simulations. Overall, in most cases, the model correctly predicts quantitatively different measured parameters, particularly for shorter (<5 min) time scales, indicating that the set of constants and stoichiometries used in the model describe the system well. This result also supports the view that partitioning of Δψ and ΔpH by ion movements is important for controlling photosynthetic responses[9,16,32,43]. It is noteworthy that the model requires the involvement of cyclic electron transport for proper description of the measured data. Without implementation of cyclic electron transport the model failed to predict the experimental qL, ΦII and NPQ data (Supplementary Fig. 7, compare with Fig. 3b that includes cyclic electron transport).

Impact of KEA3, VCCN1 and ClCe activities on ion fluxes and thylakoid membrane energization. Computer modelling allows deciphering of the individual contributions of ion transporter/channels on fluxes of Cl^- and K^+ as well on membrane energization. Because the model predicts measured parameters more accurately over the first minutes of illumination, we decided to study ion fluxes, ΔpH and Δψ over the first 5 minutes only. This restriction to shorter periods is further justified by the fact that ion transporter/channel mutants show most pronounced phenotypes under fluctuating light conditions[23,32,33]; that is, when fast changes are required. Channel/transporter independence analysis in the higher-order mutants justifies analyses of KEA3, VCCN1 and ClCe individually over the first minutes of illumination to understand how they work in concert. In line with data from other groups[26,27], the *clce* loss-of-function mutant phenotype is very weak for the conditions examined here (Supplementary Fig. 8b). Therefore, the following analyses focus on the impact of VCCN1 and KEA3 only, which reduces the complexity of the system without compromising essential aspects of ion fluxes across the thylakoid membrane. Figure 4b

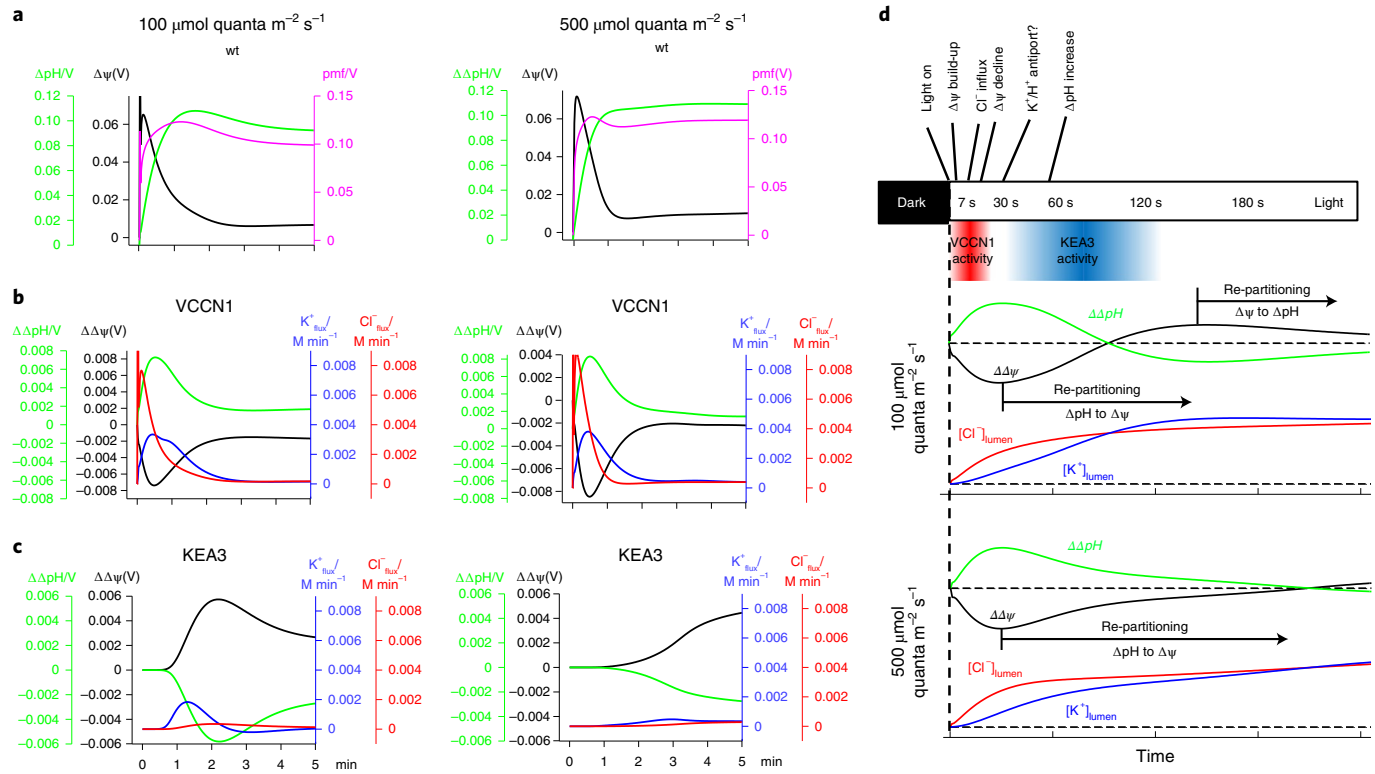

Fig. 4 | Specific role of KEA3 and VCCN1 for thylakoid energization and ion fluxes calculated from our mathematical model. a, Light-induced changes (left, 100 µmol quanta m^{-2} s^{-1}; right, 500 µmol quanta m^{-2} s^{-1}) in proton concentration in the lumen (green), Δψ (black) and pmf (purple) in WT plants. The kinetics represent the first 5 minutes of illumination. **b**, Specific changes induced by the Cl^- channel VCCN1. Data show the simulated differences of WT minus *vccn1*, that is they express VCCN1-induced changes in WT plants. **c**, Specific changes induced by the K^+ channel KEA3. **d**, The upper panel represents the time series of events after the light was turned on. The middle and lower panels show calculated differences in membrane energization and ion concentrations between WT and *vck* (WT minus *vck*), that is the kinetics reveal changes caused by the ion transporters/channels (VCCN1, KEA3 and ClCe) as they occur in WT plants for the two light intensities. ΔΔpH are expressed in *V* units (ΔΔpH × 0.060) to allow better comparison with Δψ.

(VCCN1) and Fig. 4c (KEA3) show differences for WT minus mutant, that is it reports specifically on the function of the anion channel or K^+/H^+ antiporter in WT plants.

VCCN1. The Cl^- channel VCCN1 was modelled as a resistor-like channel (Supplementary Methods), with its response to electrochemical potential (Cl^-) fit to in vitro observations described in an earlier study[25]. During the first seconds of illumination with 100 µmol quanta m^{-2} s^{-1}, Δψ rose steeply (peak ~7 s, Fig. 4a left panel) leading to activation of the voltage-gated VCCN1 channel. The resulting Cl^- influx also peaks at ~7 s (red curve in Fig. 4b) indicating the causal link between Δψ and Cl^- fluxes, that is Δψ dissipation involves mainly VCCN1 during the first minute of illumination. The VCCN1-specific Δψ relaxation (Fig. 4b black) was accompanied by a build-up of the ΔpH component seen as antiparallel behaviour of ΔΔψ (black curve) and ΔΔpH (green curve) in Fig. 4b peaking at ~30 s. The kinetics of VCCN1-mediated ion fluxes are similar at 500 µmol quanta m^{-2} s^{-1} (right panel in Fig. 4b) but the amplitudes of these fluxes were more intense at higher light intensities.

KEA3. KEA3 was modelled as a proton/potassium antiporter the activity of which is regulated by NADPH (we used qL as a proxy for NADPH level) and the pH_{Lumen} in accordance with the literature (Supplementary Methods). In contrast to VCCN1, the simulated behaviour for KEA3 was strikingly different (Fig. 4c). No notable KEA3-specific changes were apparent over the first minute of illumination, in a time when most VCCN1-dependent changes take place. Furthermore, in contrast to VCCN1, the kinetics of KEA3-induced changes are light-intensity dependent. At 100 µmol quanta m^{-2} s^{-1} alterations in ion fluxes in *kea3* were more rapid compared with 500 µmol quanta m^{-2} s^{-1} (see also Fig. 1). We first focus on 100 µmol quanta m^{-2} s^{-1}. KEA3-mediated K^+ influx peaks at ~78 s (blue curve Fig. 4c) in parallel to the ΔpH build-up (Fig. 4a), which is expected for a proton-driven K^+ import by KEA3. The K^+/H^+ antiport activity leads to a decline in ΔpH (Fig. 4c green curve) paralleled by an increase in the Δψ component (Fig. 4c black curve), that is a re-partitioning from ΔpH to Δψ occurring between 1 and 2 min. However, after ΔpH and Δψ reached their extrema (~2 min), the activity of KEA3 decreases, probably as a result of ATP synthase activation and its impact on ΔpH[43]. This leads to a relaxation of ΔpH and Δψ at around 10 min (see ΔNPQ for *k* in Fig. 1a). Similar to VCCN1, the antiparallel ΔpH/Δψ changes mediated by KEA3 are almost simultaneous. At 500 µmol quanta m^{-2} s^{-1} KEA3-mediated K^+ influx into the lumen activates later and lower (Fig. 4c right, blue line) although the initial ΔpH increase is similar to that for 100 µmol quanta m^{-2} s^{-1} (compare green curves in Fig. 4a, right with left). The lack of activity of KEA3 at 500 µmol quanta m^{-2} s^{-1} indicates regulatory inactivation of this transporter at higher light intensity (see below). The slow and weak KEA3 activation leads to decreased and slower re-partitioning from ΔpH to Δψ (Fig. 4c right).

Employing the predictive power of the computer model. *KEA3 regulation*. Figure 4c reveals low KEA3 activity at 500 µmol quanta m^{-2} s^{-1}, but not at 100 µmol quanta m^{-2} s^{-1}. This is unexpected because

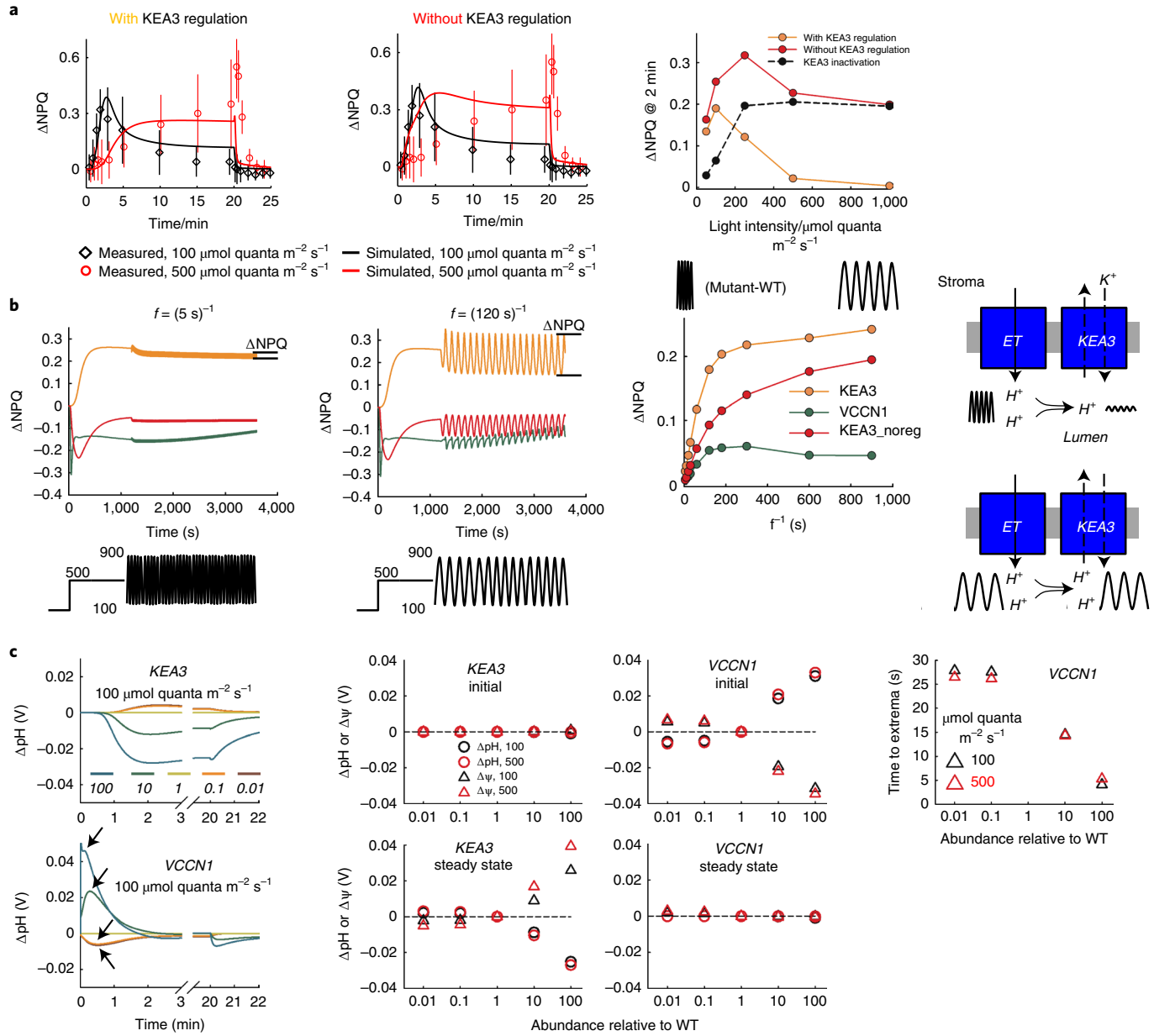

Fig. 5 | Computer simulation for the functional characterization and regulation of KEA3 and VCCN1. a, Comparison between measured (circles) and simulated (lines) ΔNPQ (mutant minus WT) data for 20 min of illumination at two different light intensities. Redox-dependent downregulation of KEA3 activity is required for 500 μmol quanta m^{-2} s^{-1} (left graph, red line and symbols). KEA3 inactivation (right graph, black curve) derived as the difference between ΔNPQ with (orange) and without KEA3 (red) regulation. **b**, Dependence of VCCN1 and KEA3 ion fluxes expressed as ΔNPQ on sinusoidal changes in light intensities. The two graphs on the left show examples for high (left) and low (right) frequencies responses for KEA3 (orange), KEA3 without redox-regulation (red) and VCCN1 (green). The plots at the bottom show the light protocol. Numbers indicate light intensities in μmol quanta m^{-2} s^{-1}. The amplitudes of the ΔNPQ response for the two frequencies are indicated by black horizontal lines for KEA3. The graph on the right gives a detailed dependence of ΔNPQ on the frequency of the fluctuating light. The panel on the far right illustrates how the antiporter activity of KEA3 responds to faster (top) and slower (bottom) changes in light intensities/proton pumping into the lumen. ET, electron transport chain. **c**, Response of ΔpH and Δψ to different abundances of VCCN1 and KEA3. The two graphs on the left show examples of ΔpH responses if the transporter/channel concentration changes from 0.01- to 100-fold of the WT level. Black arrows for VCCN1 indicate a shift in the ΔpH extrema. The middle plots show ΔpH and Δψ changes as function of KEA3 and VCCN1 abundances for 100 (black symbols) and 500 (red symbols) μmol quanta m^{-2} s^{-1}. The graphs on the upper panel illustrate initial pH/Δψ changes (from 0 s to 50 s), the plots in the lower panel illustrate steady-state changes (20 min of illumination). The graph on the right shows how the time point of the early ΔpH (Δψ) spike (black arrows in the graph to the bottom left) shifts as function of VCCN1 concentration in thylakoid membranes.

the driving force for H^+/K^+ antiport at 500 μmol quanta m^{-2} s^{-1} is even higher than at 100 μmol quanta m^{-2} s^{-1} (see ΔpH in Fig. 4a). This observation points to a downregulation of KEA3 activity at higher light intensities. Recent studies provide evidence for KEA3 regulation via a so-called KTN domain located at the C-terminus of the antiporter[44,45]. For the bacterial KEA3 homologue KefC it was shown that the regulatory KTN domain binds $NAD(P)^+/NAD(P)H$[46]. The reduced coenzyme has an inhibitory effect on the transport activity. Recently, independent studies in planta showed that the KTN domain of KEA3 extents into the stroma[44,47] where the

Table 1 | Impact on enzymatic parameters of KEA3 on NPQ determined by the computer model

pK_a Hill	5.5	6.0	6.5
1	28 s 1.94	25 s 1.85	23 s 1.77
3	28 s 1.91	24 s 1.80	22 s 1.70
5	28 s 1.89	24 s 1.77	22 s 1.66

Conditions: Illumination for 60 min with 500 µmol quanta m^{-2} s^{-1} followed by change to 100 µmol quanta m^{-2} s^{-1}. The upper number in each cell represents the time constant for NPQ relaxation after the light-intensity switch. The second number gives the steady-state NPQ value for 500 µmol quanta m^{-2} s^{-1} at the end of the 60-min period. The time constant was determined by bi-exponential fitting of the NPQ relaxation curve. The time represents the dominating fast relaxation component (amplitude 75–81%).

NADP(H) pools vary according to the photosynthetic status of the chloroplast. It is therefore likely that elevated NADPH/NADP ratios at higher light intensities downregulate KEA3 activity[44,47]. To test this, we ran simulations with or without NADPH-dependent downregulation of KEA3 activity at different light intensities. Comparison with measured ΔNPQ data shows clearly that NADPH-triggered downregulation is required to explain experimental results at 500 µmol quanta m^{-2} s^{-1} but that this regulation is not required for 100 µmol quanta m^{-2} s^{-1} (Fig. 5a, for other mutants see Supplementary Fig. 9). A detailed light-intensity dependency of the downregulation of KEA3 activity (black curve, Fig. 5a, right) derived from the difference of ΔNPQ in the presence (orange) and absence (red) of KEA3 regulation reveals a steady inactivation of the antiporter with increasing light intensity reaching a plateau at 250 µmol quanta m^{-2} s^{-1}.

Furthermore, the model allows for the study of functional implications if regulatory parameters of KEA3 were altered. Table 1 summarizes changes in NPQ for different pK_a values for the pH_{Lumen}-dependent activation of the antiporter and for different Hill coefficients for the reductive inactivation of KEA3 by NADPH. Changing the pK_a values for KEA3 from 5.5 to 6.5 leads to an ~20% acceleration in NPQ relaxation (from 28 s to 22 s), whereas changes in the Hill coefficient for NADPH-triggered inactivation has no apparent impact on the speed of NPQ kinetics. Alteration of the Hill coefficient has a small impact on the steady-state NPQ, whereas increasing the pK_a value leads to a ~10% decrease in NPQ. The results presented in Table 1 demonstrate that modulation of the sensitivity of KEA3 to pH_{Lumen} or to NADPH-dependent downregulation has only minor functional consequences.

KEA3 and VCCN1 under fluctuating light. A second application of the computer model is to determine how fast KEA3 and VCCN1 activities respond to fluctuating (sinusoidal) light intensities. To this end, the simulation started with a 20-min pre-illumination period to activate the Calvin–Benson cycle followed by sinusoidal changing light intensities alternating between 100 and 900 µmol quanta m^{-2} s^{-1} over a further 40-min period (Fig. 5b, bottom). Figure 5b gives the ΔNPQ (mutant minus WT) for different frequencies of fluctuating light intensities. The two examples for high ($f=(5\,s)^{-1}$, left) and low ($f=(120\,s)^{-1}$, middle) frequencies demonstrate that the loss of KEA3 activity has a substantial impact on the fluctuating light response only for lower frequencies, but not if the light intensity changes faster. This is visualized by the changes in ΔNPQ amplitudes in response to the sinusoidal light fluctuations for the two frequencies (indicated in Fig. 5b). The frequency dependency of ΔNPQ in Fig. 5b (right) derived from this analysis monitors the frequency dependency of KEA3 and VCCN1 activities. It indicates that only if the fluctuation in light intensity and therefore proton pumping into the lumen is slow enough does the lack of H^+/K^+ antiport in the *kea3* mutant lead to a ΔNPQ tuning phenotype (see panel to the far right in Fig. 5b). The change in VCCN1 amplitude is relatively small but that for KEA3 is notable (ΔNPQ > 0.2). Figure 5b (right) reveals that half of KEA3 antiport activity is reached at a frequency of ~$(60\,s)^{-1}$. Repeating this analysis with a KEA3 transport version without NADPH regulation shows that this leads to a less-efficient response over the entire frequency domain, that is this unregulated KEA3 version becomes a slow responding antiporter to fluctuating light.

Impact of KEA3 and VCCN1 abundances on thylakoid energetics. The mode of action of KEA3 and VCCN1 allows prediction of how changes in their relative abundance will impact ΔpH, Δψ, NPQ and electron transport. In contrast to these more intuitive predictions, the magnitude of changes in these parameters in response to changes in antiporter and channel concentrations in the thylakoid membrane is not straightforward. Figure 5c shows how ΔpH changes if KEA3 or VCCN1 abundances vary between 0.01 and 100 times WT levels (mutant minus WT) for a light intensity of 100 µmol quanta m^{-2} s^{-1}. As expected (see above), an increase in KEA3 levels leads to a decrease in ΔpH with a lag time of ~1 min, whereas an increase in VCCN1 abundance has the opposite effect, mainly at shorter times. These alterations in ΔpH and Δψ are analysed quantitatively in Fig. 5c (middle) for early time points ('initial' between 0 s and 50 s after light on) or for steady-state conditions (20 min light on). The analysis was performed for 100 (black symbols) and 500 (red symbols) µmol quanta m^{-2} s^{-1}. The reduction in KEA3 and VCCN1 abundances (0.1- and 0.01-fold) has a moderate effect on the pmf components. However, higher concentrations of KEA3 and VCCN1 lead to much larger changes in ΔpH and Δψ (in opposite directions). Note that ΔpH changes are expressed in volts, for example a change in −0.03 V as seen for 100-fold higher KEA3 abundance translates into a ΔpH change of ~0.5 pH units or an NPQ decrease of an impressive 1.5 units (Supplementary Fig. 10). A similar change in ΔpH, Δψ, NPQ magnitudes are apparent for 10- and 100-fold increases in VCCN1 concentrations but in opposite directions and only for illumination times <30 s. An additional implication of changing the VCCN1 abundance in thylakoid membranes is that the position of the ΔpH/Δψ spike (black arrows in Fig. 5c, bottom left) shifts to shorter times if VCCN1 concentration increases (Fig. 5c, right). Changing VCCN1 from 0.1-fold to 100-fold accelerates the ΔpH/Δψ response (spike) from ~27 s to ~5 s independent of light intensity.

Discussion

Temporal sequence of events unravelled by mutant analysis and mathematical modelling. In this study, we demonstrated that our extended mathematical model was able to describe a range of measured parameters (Fig. 3), as well as functional consequences for mutants that affect ion homoeostasis around thylakoid membranes. The model allows deciphering of an order of events that is summarized in Fig. 4d for two light intensities. The data show differences between WT minus the *vck* triple mutant, which indicate how the concerted action of the three ion channels/transporters fine-tune the pmf through ion fluxes. At a growth light intensity of 100 µmol quanta m^{-2} s^{-1} the fast build-up of Δψ triggers Cl^- influx by the voltage-gated VCCN1 into the lumen leading to partitioning of the pmf from Δψ to ΔpH. This initial partition phase is completed after ~30 s. At this point, the ΔpH rise is half-maximal (Fig. 4a, green curve) leading to activation of KEA3 and re-partitioning from Δψ to ΔpH that is completed after ~120 s. This is followed by a slower secondary re-partitioning phase from ΔpH to Δψ. Thus, the concerted actions of VCCN1 and KEA3 lead to oscillations in the Δψ and ΔpH components of the pmf. Physiologically these oscillations make sense because during the initial phase of illumination

the build-up of the ΔpH provides well-needed photoprotection via NPQ and photosynthetic control. Additionally, ΔpH build-up helps to activate ATP synthesis via ATP synthase by protonation of luminal amino acids[48]. After the initial period, a re-partition from ΔpH into Δψ allows faster electron transport by releasing the NPQ brake and photosynthetic control; that is, light is now converted more efficiently, which is beneficial under low light conditions. Figure 4d shows that an important contributor for these ΔpH/Δψ oscillations is the ratio of Cl^- to K^+ concentrations in the thylakoid lumen controlled by VCCN1 and KEA3 activities. Inspection of Fig. 4d at both light intensities shows that ΔpH increases and Δψ decreases if the change in Cl^- concentration is higher than the change in K^+ and vice versa. Consequently, at crossing points of ion concentrations the changes in both pmf components are also equal (compare cross points of red/blue and black/green lines in Fig. 4d). Overall Fig. 4d demonstrates relative fast changes in ion concentrations, and as a consequence pmf partitioning, that explain why phenotypes of thylakoid membrane ion transport/channel mutants are more apparent under fluctuating light (Supplementary Fig. 3, refs. [25,33,49]). In contrast to 100 µmol quanta m^{-2} s^{-1}, re-partitioning from ΔpH to Δψ is much slower at 500 µmol quanta m^{-2} s^{-1}; that is, the Δψ /ΔpH crossing point is shifted from ~90 s to ~210 s (Fig. 4d). This delay in ΔpH relaxation could help to photoprotect the system using NPQ/photosynthetic control at this higher light intensity. Mechanistically, the slower ΔpH relaxation at 500 µmol quanta m^{-2} s^{-1} can be explained by the low activity of KEA3 (see K^+ flux in Fig. 4c right, blue line) caused by downregulation of the antiporter (see below).

Insights in KEA3 and VCCN1 operation. *Defining design strategies for thylakoid ion transporter/channels.* The power of our experientially validated computer model was explored for deeper physiological characterization of KEA3 and VCCN1 that is difficult to access experimentally. The analyses shown in Fig. 5a provide strong evidence for redox-dependent downregulation of KEA3, probably by NADPH, at higher light intensities in line with indications from the literature[44,45]. The light-intensity dependence of KEA3 inactivation reveals that 50% inactivation is reached at ~100 µmol quanta m^{-2} s^{-1}; that is, the regulation of antiport activity is tuned around the growth light intensity. Further insights into KEA3 and VCCN1 operation are provided by their frequency dependency (Fig. 5b). For both VCCN1 and KEA3, a full response to sinusoidal modulated light intensities in light-adapted plants is only apparent at frequencies lower than ~$(100\,s)^{-1}$. This might reflect a limited capacity for ion transport, in particular for KEA3; that is, if the proton pumping into the lumen by electron transport fluctuates too fast a limiting capacity of KEA3 leads to a damping of the proton oscillation and the NPQ response. It is noteworthy that these results are exclusively caused by KEA3 and VCCN1 and not by pleiotropic effects that are possible in real mutant studies. This is a clear advantage of computer simulations. The analysis in Fig. 5b highlights the importance of redox-regulation of KEA3 activity under fluctuating light. A lack thereof would make the H^+/K^+ antiporter slower and less responsive to fluctuating light intensities. Further analyses reveal that the biggest impact on thylakoid membrane energetics can be achieved by overexpressing VCCN1 and KEA3 but not by adjusting enzymatic parameters of KEA3 (Table 1). The latter has only a minor impact on NPQ. The overexpression simulation shows an intriguing high sensitivity of Δψ, ΔpH and NPQ on higher concentrations of KEA3 and VCCN1. Furthermore, increasing VCCN1 abundance also accelerates the transient and early ΔpH spike. The results of our analyses may guide genetic engineering strategies to adjust thylakoid energization to optimize and fine-tune energy transduction in plants. In this context, the extended computer program presented in this study can be employed to help develop custom-made plants with certain bioenergetic features by uncovering and exploring non-intuitive behaviours of thylakoid membrane components.

Conclusion

Our computer simulations reveal that the different kinetic behaviours of VCCN1 and KEA3 and the accompanied ion fluxes determine mutual oscillatory increases and decreases in ΔpH and Δψ across thylakoid membranes required for the light-dependent control of electron transport and photoprotection at the onset of illumination. Furthermore, detailed characterization of KEA3 activity shows that the redox-dependent (NADPH) downregulation of KEA3 activity regulates NPQ and membrane energization around growth light intensities and enhances the response to fast changing fluctuating light intensities, a feature that is relevant for efficient plant growth in natural environments. In contrast, membrane energization and NPQ are relatively insensitive to the precise values of enzymatic KEA3 parameters that determine its regulatory power (pK_a of activation, Hill coefficient for downregulation). However, increasing VCCN1 and KEA3 abundance in thylakoid turned out to be a powerful way to tune photoprotection and electron transport.

Methods

Plant materials and growth conditions. *Arabidopsis thaliana* WT (Col-0) and confirmed mutant seeds were sown on soil, and plants were maintained in a growth chamber at a constant temperature of 21 °C, and 9 h illumination per day at 120 µmol m^{-2} s^{-1}. Double mutants were acquired by crossing corresponding single mutants: *kea3-1* (ref. [23]), *vccn1-1* (SALK_103612C) and *clce-2* (Salk_010237). The triple mutant was obtained by crossing *kea3-1clce-2* with *vccn1*. Homozygous mutants were identified using a polymerase chain reaction with genomic DNA (Supplementary Fig. 1).

Phenomics. Plants that were 4 weeks old were moved to phenomic chambers with the same photoperiod and temperature settings as in the growth chamber. After a 2–7-day acclimation period, Chl fluorescence parameters were measured at night after >2 h of dark adaptations. Data from the constant light phenomic chamber was acquired using the Fluorcam system (PSI Co.). Data from the fluctuating light phenomic chamber was acquired using PhenoCenter (LemnaTec). In the PhenoCenter during the day, after 20 min constant light at 120 µmol m^{-2} s^{-1}, light intensity was set to fluctuate every 1 min, randomly among 50, 120, 250, 400 µmol m^{-2} s^{-1} with an overall frequency of 0.6, 0.2, 0.1, 0.1 respectively, which ensured the average light intensity was close to 120 µmol m^{-2} s^{-1}.

Isolation of chloroplasts thylakoid membranes. Chloroplast and thylakoid membrane isolations were done as described in a previous study[50]. Thylakoid membranes were used for gel electrophoresis and western blotting, whereas isolated chloroplasts were used for in vitro 9-AA fluorescence measurement.

Gel electrophoresis and western blotting. Isolated thylakoids were loaded on a 10% Tris–Tricine acrylamide gel (2 µg/lane for western blotting and 4 µg/lane for Coomassie blue staining). For western blotting, gels were wet blotted onto a methanol-activated PVDF membrane (0.45 µm, Millipore). Blocking was done in 5% milk (Bio-Rad) in Tris-Buffered Saline with Tween20 buffer (pH 7.6) for 1 h at room temperature. Incubation with primary antibody raised against PsbS protein (kind gift from K.K. Niyogi, UC Berkeley, CA, USA) was done overnight in a cold room (dilution 1:2000). Secondary antibody anti-rabbit horseradish peroxidase-conjugated from donkey as a host animal (GE Healthcare) was incubated at room temperature for 2 h (dilution 1:50 000, Amersham, GE). Chemiluminescence (ECL) was recorded on Amersham Hyperfilm (GE) using Amersham ECL Western Blotting Detection Kit (GE).

9-AA fluorescence. 9-AA fluorescence kinetics was recorded with excitation at 405 nm (bandwidth 1 nm) and emission at 460 nm (bandwidth 7.5 nm). Isolated chloroplasts with 40 µg Chl were added to 1 ml of shock buffer (25 mM HEPES, 7 mM $MgCl_2$, 40 mM KCl, pH 7.8 with KOH) in a reaction cuvette with constant stirring for ~1 min followed by addition of 1 ml of double concentration buffer (25 mM HEPES, 7 mM $MgCl_2$, 260 mM KCl, 200 mM sorbitol, pH 7.8 with KOH). After ~1 min, 2 µl of 5 mM 9-AA were added before turning on the external light source following a stabilized fluorescence signal. Three minutes of illumination was followed by 2 min of dark relaxation. ΔpH was calculated as described by Van et al.[51].

Pigments analysis. Leaf samples illuminated under 500 µmol m^{-2} s^{-1} light for 20 min were frozen in liquid N_2 before carotenoid extraction in 100% ethanol on ice. Extracted pigments were stored at −20 °C and analysed using reverse-phase high-performance liquid chromatography within 24 hours[52].

Chl fluorescence measurements. Before light adaptation, the minimum fluorescence (Fo) and maximum fluorescence (Fm) were determined. For

light-adapted leaves the steady-state fluorescence level (Fs) and maximal fluorescence (Fm′) were measured and the following parameters calculated:[53] Fv/Fm = (Fm − Fo)/Fm; ΦII = (Fm′ − Fs)/Fm′; NPQ = (Fm − Fm′)/Fm′; qL = ((Fm′ − Fs)/(Fm′ − Fo′)) × (Fo/Fs).

Difference absorption spectroscopy. Cyt b_6f complex and PSII concentrations in thylakoid membranes were derived from chemical difference absorption spectra that quantify cyt b_6 and cyt f (for cyt b_6f complex) and cyt b_{559} (for PSII). Signals were recorded using a Hitachi U3900 spectrometer (2-nm slit width, 530–580 nm). For details see ref. [54].

ECS. The ECS signals at 520 and 545 nm were measured on dark-adapted plants. The dark interval relaxation kinetics was recorded after illuminating a leaf at 500 µmol quanta m^{-2} s^{-1} light for a period (1, 2, 3, 5, 10, 19.5 min). Eight plants were used for each genotype. The ΔpH and Δψ components were calculated as described in ref. [29].

Modelling. The photosynthetic light reaction was modelled by modifying a previously described model[9]. Key improvements involve a close match between the simulated data and measured data from leaf samples. Detailed updates and explanations are available in Supplementary Methods.

Reporting Summary. Further information on research design is available in the Nature Research Reporting Summary linked to this article.

Data availability

The data sets generated during and/or analysed during the current study are available from the corresponding author on reasonable request.

Code availability

The computer code for our model is available online. A link is provided in Supplementary Information.

Received: 29 April 2020; Accepted: 18 May 2021;
Published online: 17 June 2021

References

1. Mitchell, P. Coupling of photophosphorylation to electron and hydrogen transfer by a chemiosmotic type of mechanism. *Nature* **191**, 144–148 (1961).
2. Williams, R. J. P. Possible functions of chains of catalysts. *J. Theor. Biol.* **1**, 1–13 (1961).
3. Williams, R. J. P. Possible functions of chains of catalysts II. *J. Theor. Biol.* **3**, 209–220 (1962).
4. Witt, H. T. Energy conversion in the functional membrane of photosynthesis. Analysis by light pulse and electric pulse methods: the central role of the electric field. *Biochim. Biophys. Acta* **505**, 355–427 (1979).
5. Bulychev, A. A. & Vredenberg, W. J. Light-triggered electrical events in the thylakoid membrane of plant chloroplasts. *Physiol. Plant.* **105**, 577–584 (1999).
6. Kramer, D. M., Cruz, J. A. & Kanazawa, A. Balancing the central roles of the thylakoid proton gradient. *Trends Plant Sci.* **8**, 27–32 (2003).
7. Allorent, G. et al. Global spectroscopic analysis to study the regulation of the photosynthetic proton motive force: a critical reappraisal. *Biochim. Biophys. Acta Bioenerg.* **1859**, 676–683 (2018).
8. Klughammer, C., Siebke, K. & Scheiber, U. Continuous ECS-indicated recording of the proton-motive charge flux in leaves. *Photosynth. Res.* **117**, 471–487 (2013).
9. Davis, G. A., Rutherford, A. W. & Kramer, D. M. Hacking the thylakoid proton motive force for improved photosynthesis: modulating ion flux rates that control proton motive force partitioning into Δψ and ΔpH. *Philos. Trans. Roy. Soc. B* **372**, 20160381 (2017).
10. Avenson, T., Cruz, J. A. & Kramer, D. Modulation of energy dependent quenching of excitons (qE) in antenna of higher plants. *Proc. Natl Acad. Sci. USA* **101**, 5530–5535 (2004).
11. Rumberg, B. & Siggel, U. pH changes in the inner phase of the thylakoids during photosynthesis. *Z. Naturwiss* **56**, 130–132 (1969).
12. Kobayashi, Y., Inoue, Y., Shibata, K. & Heber, U. Control of electron flow in intact chloroplasts by intathylakoid pH, not by the phosphorylation potential. *Planta* **146**, 481–486 (1979).
13. Ruban, A. V. Light harvesting control in plants. *FEBS Lett.* **592**, 3030–3039 (2018).
14. Li, Z., Wakao, S., Fischer, B. B. & Niyogi, K. K. Sensing and responding to excess light. *Annu. Rev. Plant Biol.* **60**, 239–260 (2009).
15. Pinnola, A. & Bassi, R. Molecular mechanisms involved in plant photoprotection. *Biochem. Soc. Trans.* **46**, 467–482 (2018).
16. Armbruster, U., Correa Galvis, V., Kunz, H. H. & Strand, D. D. The regulation of the chloroplast proton motive force plays a key role for photosynthesis in fluctuating light. *Curr. Opin. Plant Biol.* **37**, 56–62 (2017).
17. Demmig, B. & Gimmler, H. Properties of the isolated intact chloroplast at cytoplasmic K^+ concentrations in spinach chloroplasts. *Plant Physiol.* **73**, 169–174 (1983).
18. Robinson, S. P. & Downtown, W. J. Potassium, sodium, and chloride content of isolated intact chloroplasts in relation to ionic compartmentation in leaves. *Arch. Biochem. Biophys.* **228**, 197–206 (1984).
19. Schonknecht, G., Hederich, R., Junge, W. & Raschke, K. A voltage-dependent chloride channel in the photosynthetic membrane of a higher plant. *Nature* **336**, 589–592 (1988).
20. Enz, C., Steinkamp, T. & Wagner, R. Ion channels in the thylakoid membrane (a patch-clamp study). *Biochim. Biophys. Acta* **1143**, 67–76 (1993).
21. Finazzi, G. et al. Ion channels/trasnporters and chloroplast regulation. *Cell Calcium* **58**, 86–97 (2015).
22. Spetea, C. et al. An update on the regulation of photosynthesis by thylakoid ion channels and transporters in *Arabidopsis*. *Physiol. Plant.* **161**, 16–27 (2017).
23. Kunz, H. H. et al. Plastidial transporters KEA1, -2, and -3 are essential for chloroplast osmoregulation, integrity, and pH regulation in *Arabidopsis*. *Proc. Natl Acad. Sci. USA* **111**, 7480–7485 (2014).
24. Duan, Z. et al. A bestrophin-like protein modulates the proton motive force across the thylakoid membrane in *Arabidopsis*. *J. Integr. Plant Biol.* **58**, 848–858 (2016).
25. Herdean, A. et al. A voltage-dependent chloride channel fine-tunes photosynthesis in plants. *Nat. Commun.* **7**, 11654 (2016).
26. Herdean, A. et al. The *Arabidopsis* thylakoid chloride channel AtCLCe functions in chloride homeostasis and regulation of photosynthetic electron transport. *Front. Plant Sci.* **7**, 115 (2016).
27. Marmagne, A. et al. Two members of the *Arabidopsis* CLC (chloride channel) family, ATCLCe and AtCLCf, are associated with thylakoid and Golgi membranes, respectively. *J. Exp. Bot.* **58**, 3358–3393 (2007).
28. Carraretto, L. et al. A thylakoid-located two-pore K^+ channel controls photosynthetic light utilization in plants. *Science* **342**, 114–118 (2013).
29. Höhner, R. et al. Photosynthesis in *Arabidopsis* is unaffected by the function of the vacuolar K^+ channel TPK3. *Plant Physiol.* **180**, 1322–1335 (2019).
30. Jaslan, D. et al. Voltage-dependent gating of SV channel TPC1 confers vacuole excitability. *Nat. Commun.* **10**, 2659 (2019).
31. Tang, R.-J. et al. A calcium signalling network activates vacuolar K^+ remobilization to enable plant adaptation to low-K environments. *Nat. Plants* **6**, 384–393 (2020).
32. Dukic, E. et al. K^+ and Cl^- channels/transporters independently fine-tune photosynthesis in plants. *Sci. Rep.* **9**, 8639 (2019).
33. Armbruster, U. et al. Ion antiport accelerates photosynthetic acclimation in fluctuating light environments. *Nat. Commun.* **5**, 5439 (2014).
34. Wang, C. & Shikanai, T. Modification of activity of the thylakoid H^+/K^+ antiporter KEA3 disturbs ΔpH15 dependent regulation of photosynthesis. *Plant Physiol.* **181**, 762–773 (2019).
35. Tian, L. et al. pH dependence, kinetics and light-harvesting regulation of nonphotochemical quenching in *Chlamydomonas*. *Proc. Natl Acad. Sci. USA* **116**, 8320–8325 (2019).
36. Takizawa, K., Cruz, J. A. & Kramer, D. M. Depletion of stromal inorganic phosphate induces high 'energy-dependent' antenna exciton quenching (qE) by decreasing proton conductivity at CFO-CF1 ATP synthase. *Plant Cell Environ.* **31**, 235–243 (2008).
37. Cruz, J. A., Sacksteder, C. A., Kanazawa, A. & Kramer, D. M. Contribution of electric field (Δψ) to steady-state transthylakoid proton motive force (pmf) in vitro and in vivo. Control of pmf parsing into Δψ and ΔpH by ionic strength. *Biochemistry* **40**, 1226–1237 (2001).
38. Bailleul, B., Cardol, P., Breyton, C. & Finazzi, G. Electrochromism: a useful tool to study algal photosynthesis. *Photosynth. Res.* **106**, 179–189 (2010).
39. Schuldiner, S., Rottenberg, H. & Avron, M. Determination of ΔpH in chloroplasts. 2. Fluorescent amines as a probe for the determination of ΔpH in chloroplasts. *Eur. J. Biochem.* **25**, 64–70 (1972).
40. Johnson, M. P., Zia, A. & Ruban, A. V. Elevated ΔpH restores rapidly reversible photoprotective energy dissipation in *Arabidopsis* chloroplasts deficient in lutein and xanthophyll cycle activity. *Planta* **235**, 193–204 (2011).
41. Jahns, P. & Holzwarth, A. R. The role of the xanthophyll cycle and of lutein in photoprotection of photosystem II. *Biochim. Biophys. Acta* **1817**, 182–193 (2012).
42. Nielkens, M. et al. Idnetification of a slowly inducible zeaxanthin-dependent component of non-photochemical quenching of chlorophyll fluorescence generated under steady-state conditions in *Arabidopsis*. *Biochim. Biophys. Acta* **1797**, 466–475 (2010).
43. Correa Galivs, V. et al. H^+ transport by K^+ exchange antiporter3 promotes photosynthesis and growth in chloroplast ATP synthase mutants. *Plant Physiol.* **182**, 2126–2142 (2020).
44. Wang, C. et al. Fine-tuned regulation of the K^+/H^+ antiporter KEA3 is required to optimize photosynthesis during induction. *Plant J.* **89**, 540–553 (2017).
45. Armbruster, U. et al. Regulation and levels of the thylakoid K^+/H^+ antiporter KEA3 shape the dynamic response of photosynthesis in fluctuating light. *Plant Cell Physiol.* **57**, 1557–1567 (2016).

46. Roosild, T. P. et al. KTN (RCK) domains regulate K^+ channels and transporters by controlling the dimer-hinge conformation. *Structure* **17**, 893–903 (2009).
47. Uflewski, M. et al. Functional characterization of proton antiport regulation in the thylakoid membrane. *Plant Physiol.* https://doi.org/10.1093/plphys/kiab135 (2021).
48. Gräber, P., Junesch, U. & Schatz, G. H. Kinetics of proton-transport coupled ATP synthesis in chloroplasts. Activation of the ATPase by an artificially generated ΔpH and Δψ. *Ber. Bunsenges.* **88**, 599–608 (1984).
49. Schneider, D. et al. Fluctuating light experiments and semi-automated plant phenotyping enabled by self-built growth racks and simple upgrades to the IMAGING-PAM. *Plant Methods* **15**, 156 (2019).
50. Koochak, H., Puthiyaveetil, S., Mullendore, D. L., Li, M. & Kirchhoff, H. The structural and functional domains of plant thylakoid membranes. *Plant J.* **97**, 412–429 (2019).
51. Van, T. V., Heinze, T & Rumberg, B . in *Progress in Photosynthesis Research Vol. III* (ed. Biggens J) (Martinus Nijhoff, 1987).
52. Tietz, S. et al. Functional implications of photosystem II crystal formation in photosynthetic membranes. *J. Biol. Chem.* **290**, 14091–14106 (2015).
53. Kramer, D. M., Johnson, G., Kiirats, O. & Edwards, G. E. New fluorescence parameters for the determination of QA redox state and excitation energy fluxes. *Photosynth. Res* **79**, 209–218 (2004).
54. Puthiyaveetil, S. et al. Compartmentalization of the protein repair machinery in photosynthetic membranes. *Proc. Natl Acad. Sci. USA* **111**, 15839–15844 (2014).

Acknowledgements

We thank M. Wood and Dr D. Schneider at the WSU Plant Phenomics facilities for their assistance in acquiring phenotyping data. The work was mainly supported by a US Department of Energy grant (DE-SC0017160) to H.K. and H.-H.K. Additional support from the National Science Foundation (MCB-1616982) and USDA-NIFA (#1005351 and #0119) to H.K. and by the 3rd ERA-CAPS call via the NSF PGRP programme (IOS-1847382, 1847193) to H.-H.K. and D.M.K. is acknowledged. Support for modelling work at MSU was supported by award #1847193 from the National Science Foundation. The project was also made possible thanks to a Murdock trust equipment grant (# SR-2016049) to H.-H.K. and H.K.

Author contributions

M.L., V.S., G.D. and H.-H.K. performed experiments and analysed data. M.L. G.D., D.K. H.-H.K. and H.K. designed the study. H.K. wrote the manuscript.

Competing interests

The authors declare no competing interests.

Additional information

Supplementary information The online version contains supplementary material available at https://doi.org/10.1038/s41477-021-00947-5.

Correspondence and requests for materials should be addressed to H.K.

Peer review information *Nature Plants* thanks Conrad Mullineaux, Toshiharu Shikanai and the other, anonymous, reviewer(s) for their contribution to the peer review of this work.

Reprints and permissions information is available at www.nature.com/reprints.

Publisher's note Springer Nature remains neutral with regard to jurisdictional claims in published maps and institutional affiliations.

nature research

Corresponding author(s): Helmut Kirchhoff

Last updated by author(s): May 19, 2020

Reporting Summary

Nature Research wishes to improve the reproducibility of the work that we publish. This form provides structure for consistency and transparency in reporting. For further information on Nature Research policies, see our Editorial Policies and the Editorial Policy Checklist.

Statistics

For all statistical analyses, confirm that the following items are present in the figure legend, table legend, main text, or Methods section.

n/a	Confirmed	
☐	☒	The exact sample size (*n*) for each experimental group/condition, given as a discrete number and unit of measurement
☐	☒	A statement on whether measurements were taken from distinct samples or whether the same sample was measured repeatedly
☐	☒	The statistical test(s) used AND whether they are one- or two-sided *Only common tests should be described solely by name; describe more complex techniques in the Methods section.*
☐	☒	A description of all covariates tested
☐	☒	A description of any assumptions or corrections, such as tests of normality and adjustment for multiple comparisons
☐	☒	A full description of the statistical parameters including central tendency (e.g. means) or other basic estimates (e.g. regression coefficient) AND variation (e.g. standard deviation) or associated estimates of uncertainty (e.g. confidence intervals)
☐	☒	For null hypothesis testing, the test statistic (e.g. *F*, *t*, *r*) with confidence intervals, effect sizes, degrees of freedom and *P* value noted *Give P values as exact values whenever suitable.*
☒	☐	For Bayesian analysis, information on the choice of priors and Markov chain Monte Carlo settings
☒	☐	For hierarchical and complex designs, identification of the appropriate level for tests and full reporting of outcomes
☒	☐	Estimates of effect sizes (e.g. Cohen's *d*, Pearson's *r*), indicating how they were calculated

Our web collection on statistics for biologists contains articles on many of the points above.

Software and code

Policy information about availability of computer code

Data collection	For phenotyping experiments (Fig. 1) software from the companies 'Lemnatch' (software: LemnatechPhenocenter) and 'Photon Systems Instruments' (software PSI Fluorcam7) were used. For in vivo spectroscopy a non-commercial self-written software or software from the company 'Hansatech' (software: ModFluor32) were used.
Data analysis	Microsoft Excel Version 16, Sigma Plot Version 11, Python 3.9.0

For manuscripts utilizing custom algorithms or software that are central to the research but not yet described in published literature, software must be made available to editors and reviewers. We strongly encourage code deposition in a community repository (e.g. GitHub). See the Nature Research guidelines for submitting code & software for further information.

Data

Policy information about availability of data

All manuscripts must include a data availability statement. This statement should provide the following information, where applicable:

- Accession codes, unique identifiers, or web links for publicly available datasets
- A list of figures that have associated raw data
- A description of any restrictions on data availability

The datasets generated during and/ or analyzed during the current study are available from the corresponding author on reasonable request.

Field-specific reporting

Please select the one below that is the best fit for your research. If you are not sure, read the appropriate sections before making your selection.

☒ Life sciences ☐ Behavioural & social sciences ☐ Ecological, evolutionary & environmental sciences

For a reference copy of the document with all sections, see nature.com/documents/nr-reporting-summary-flat.pdf

Life sciences study design

All studies must disclose on these points even when the disclosure is negative.

Sample size	Samples sizes were chosen based on the number of available plants.
Data exclusions	No data were excluded from analysis.
Replication	All attempts of replication were successful. Details on how often experiments were replicated are given in the figure legends.
Randomization	Individual plants were picked randomly. Plant allocation was random.
Blinding	Investigators were not blinded. Blinding was not relevant because we used unbiased data analysis tools.

Reporting for specific materials, systems and methods

We require information from authors about some types of materials, experimental systems and methods used in many studies. Here, indicate whether each material, system or method listed is relevant to your study. If you are not sure if a list item applies to your research, read the appropriate section before selecting a response.

Materials & experimental systems

n/a	Involved in the study
☐	☒ Antibodies
☒	☐ Eukaryotic cell lines
☒	☐ Palaeontology and archaeology
☒	☐ Animals and other organisms
☒	☐ Human research participants
☒	☐ Clinical data
☒	☐ Dual use research of concern

Methods

n/a	Involved in the study
☒	☐ ChIP-seq
☒	☐ Flow cytometry
☒	☐ MRI-based neuroimaging

Antibodies

Antibodies used	Secondary antibody from GE Healthcare Anti-Rabbit HPR conjugated from host donkey as a host animal (NIF824, lot: 9794849). The PsbS antibody was a kind gift of Dr. Krishna K. Niyogi (UC Berkeley, CA, USA).
Validation	Li, X.-P., Phippard, A., Pasari, J., and Niyogi, K. K. (2002) Structure-function analysis of photosystem II subunit S (PsbS) in vivo. Funct. Plant Biol. 29, 1131–1139